Odorant responses of olfactory sensory neurons expressing the odorant receptor MOR23: A patch clamp analysis in gene-targeted mice

Xavier Grosmaitre*, Anne Vassalli†, Peter Mombaerts†, Gordon M. Shepherd‡, and Minghong Ma*§

*Department of Neuroscience, University of Pennsylvania School of Medicine, Philadelphia, PA 19104; †The Rockefeller University, New York, NY 10021; and ‡Department of Neurobiology, Yale University School of Medicine, New Haven, CT 06511

Edited by Linda M. Bartoshuk, Yale University School of Medicine, New Haven, CT, and approved December 15, 2005 (received for review September 29, 2005)

A glomerulus in the mammalian olfactory bulb receives axonal inputs from olfactory sensory neurons (OSNs) that express the same odorant receptor (OR). Glomeruli are generally thought to represent functional units of olfactory coding, but there are no data on the electrophysiological properties of OSNs that express the same endogenous OR. Here, using patch clamp recordings in an intact epithelial preparation, we directly measured the transduction currents and receptor potentials from the dendritic knobs of mouse OSNs that express the odorant receptor MOR23 along with the green fluorescent protein. All of the 53 cells examined responded to lyral, a known ligand for MOR23. There were profound differences in response kinetics, particularly in the deactivation phase. The cells were very sensitive to lyral, with some cells responding to as little as 10 nM. The dynamic range was unexpectedly broad, with threshold and saturation in individual cells often covering three log units of lyral concentration. The potential causes and biological significance of this cellular heterogeneity are discussed. Patch clamp recording from OSNs that express a defined OR provides a powerful approach to investigate the sensory inputs to individual glomeruli.

olfactory receptor | olfactory epithelium | signal transduction | lyral

The detection and discriminatory power of the mammalian nose rely on ≈1,000 odorant receptors that are expressed in olfactory sensory neurons (OSNs) within the main olfactory epithelium (1–3). Axons of OSNs that express the same odorant receptor (OR) gene usually coalesce into two glomeruli of the olfactory bulb (4–6). Conversely, all axons that innervate a particular glomerulus are from OSNs that express a given OR (7). Rapid progress has been made in mapping glomerular activities by detecting odorant-evoked signals of various types: intrinsic imaging (8), 2-deoxyglucose uptake (9), calcium imaging (10), c-fos labeling (11), fMRI (12), and fluorescence of synaptopHluorin (13).

To understand how odor information is encoded and processed from the nose to the bulb, it is crucial to know how similar or dissimilar the odorant response properties are of OSNs that express the same OR and project their axons to the same glomeruli. The intermingling of ≈1,000 types of OSNs in the main olfactory epithelium precludes such investigation in wild-type animals. By genetically tagging OSNs that express the M71 or M72 OR in mice, we have previously measured calcium signals elicited by odorants in the cell bodies of dissociated cells and described the odorant response profiles of M71 or M72-expressing OSNs (14–16). Although the dynamic range of individual cells to the ligands acetophenone and benzaldehyde was narrow (one order of magnitude), the overall sensitivity of M71-expressing OSNs varied over two orders of magnitude. This approach has two drawbacks. First, enzymatic and mechanical dissociation extracts cells from their normal cellular environment. Second, odorant responses were measured in the form of calcium transients in the cell bodies, a parameter that is distal from the initial, odorant-evoked signal transduction event.

Here, we have overcome these limitations by directly measuring the transduction currents and receptor potentials by using perforated patch clamp recordings in intact, nondissociated preparations of mouse olfactory epithelium (17, 18). We investigated the electrophysiological responses of green-fluorescent cells from MOR23-IRES-tauGFP mice (19) to lyral, a previously identified odorous ligand for MOR23 (20). All of the 53 MOR23 cells responded to lyral but showed profound differences in their response kinetics and odorant sensitivity. The dynamic range was unexpectedly broad, with threshold and saturation in individual cells often covering three log units of lyral concentration. Thus, mouse OSNs that are homogeneous in terms of the expressed OR are heterogeneous in their responses to a given odorous ligand.

Results

Responses to Lyral. The strain of MOR23-IRES-tauGFP mice was constructed by gene targeting in embryonic stem cells (19). In these mice, MOR23-expressing cells can be identified in their entirety by virtue of their intense expression of tauGFP (Fig. 1*A*). The dendritic knobs and cilia of the GFP^+ cells were readily visible in our preparation of intact, nondissociated olfactory epithelium (Fig. 1*B*). The data reported in this paper were obtained from a total of 63 cells: 53 MOR23-expressing cells and 10 neighboring GFP^- cells, with "neighboring" defined as within 5 μm of a GFP^+ cell. For the GFP^+ cells, we recorded from the dendritic knobs of cells that could be identified unequivocally under differential interference contrast (DIC) observation (Fig. 1*C*). Henceforth such cells are referred to as MOR23 cells.

We measured responses to lyral, a known ligand for MOR23 (20). Two of 10 neighboring GFP^- cells showed weak responses to lyral at high concentrations ($\geq$100 μM). In contrast, 53 of 53 MOR23 cells responded to lyral, with ≈90% responding to lyral at $\leq$10 μM. Both high K^+ solution and lyral elicited inward currents under the voltage clamp mode, and depolarization under the current clamp mode (Fig. 2).

To quantify the response properties of MOR23 cells, we measured the following four parameters for each transduction current: the peak current, the response latency, the 0–90% rising time, and the half-width of the current (Fig. 3*A*). The half-width of the currents was chosen because the deactivation phase of odorant responses in most cells could not be fitted well by exponential curves (Fig. 2 *B* and *C*). Because the rising phase was relatively fast and did not vary much from cell to cell, the

Conflict of interest statement: No conflicts declared.

This paper was submitted directly (Track II) to the PNAS office.

Abbreviations: DIC, differential interference contrast; OR, odorant receptor; OSN, olfactory sensory neuron.

§To whom correspondence should be addressed. E-mail: minghong@mail.med.upenn.edu.

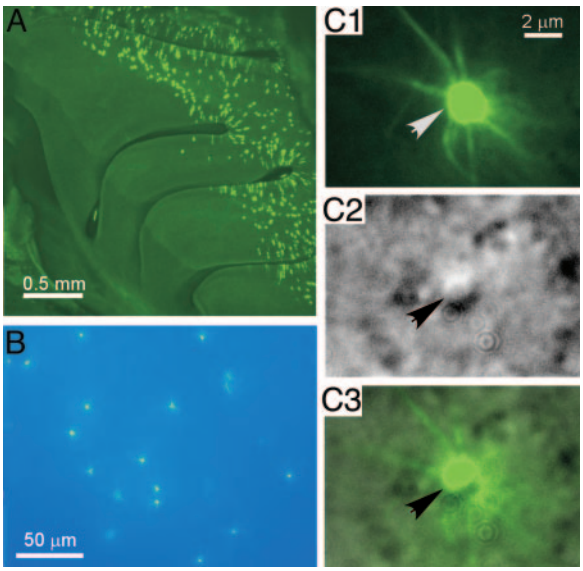

Fig. 1. Visualization of MOR23 cells under fluorescence illumination and DIC microscopy. (*A*) Whole-mount view of the nasal turbinates in a MOR23-IRES-tauGFP mouse under fluorescence illumination. (*B*) Visualization of the GFP^+ (MOR23) cells in the intact, nondissociated olfactory epithelium under fluorescence illumination. (*C*) Identification of the MOR23 cells under DIC microscopy. The same field was taken under fluorescence illumination (*C1*) or DIC (*C2*). *C3* shows an overlay of *C1* and *C2*. The arrows (in the same position in all three images) point to the knob of a MOR23 cell.

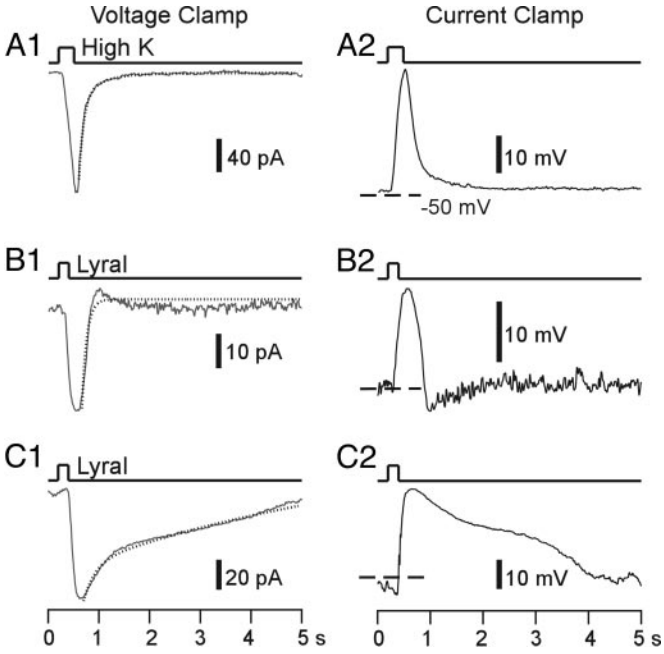

Fig. 2. MOR23 cells show heterogeneous response kinetics to lyral. Inward currents under the voltage clamp mode (*A1*, *B1*, and *C1*) or depolarizing membrane potentials under the current clamp mode (*A2*, *B2*, and *C2*) were induced by high-K^+ (*A*) or 300 μM lyral (*B* and *C*). The recordings from *A–C* were from three different cells. The holding potential was −50 mV under voltage clamp (*A1*, *B1*, and *C1*), and dashed lines indicate −50 mV under current clamp (*A2*, *B2*, and *C2*). The dotted lines in *A1*, *B1*, and *C1* are fitted double-exponential curves.

half-width of the current mainly reflected how fast the transduction current returned to the baseline.

The odorant response amplitude and kinetics in single cells changed with concentration (see below for dose–response relation). Fig. 3*B* shows the half-width of the transduction currents plotted against lyral concentration in nine cells. In one cell (filled triangles), the response to 1,000 μM was significantly larger and wider than to 100 μM; in a second cell (open circles), there was no clear trend. In the remaining seven cells, the half-width slightly increased with the concentration and became steady at near-saturating or saturating concentrations. For any given concentration, the variations among cells exceeded the changes for a single cell (except for the one in filled triangles). We therefore analyzed the responses at 100-1,000 μM to enable comparison among the recorded cells (Fig. 3 *C* and *D*). We observed that lyral-induced responses ($n = 25$ cells) showed significant differences from high K^+ responses ($n = 16$ cells) in the latency and the half-width of the transduction current but not in the peak current and the 0–90% rising time (Fig. 3*C*). We note that currents induced by lyral and high K^+ are from different sources, although their amplitudes are comparable.

Binding of the odorant molecules to ORs triggers a series of events: sequential activation of G protein and adenylyl cyclase leading to increased cAMP levels. Under voltage clamp mode, odorant stimulation elicits inward currents that are carried by the cyclic nucleotide-gated channel and the Ca^{2+}-activated Cl^- channel (21). As expected, the latencies for lyral-induced responses (164 ± 12.9 ms, mean ± SE) were much longer than those of high-K^+ responses (77 ± 5.5 ms), presumably reflecting the extra time (≈90 ms) that is needed for activating this transduction cascade; this process was similar among MOR23 cells (Fig. 2 and 3*C*).

The most obvious difference among lyral-induced responses occurs in the deactivation phase (Fig. 2 *B* and *C*), quantified by the half-width of the currents (Fig. 3*C*). Lyral responses cover a significantly wider range (402–3,768 ms) than the high-K^+ responses (279–1,679 ms; Fig. 3*D*). When fitted with the Gaussian probability distribution, lyral responses are centered at 1,529 ms with a width of 2,317 ms (variance $\sigma^2 = 1.04$), whereas high-K^+ responses centered at 825 ms with a width of 642 ms ($\sigma^2 = 0.30$). Because the amplitude of the responses also varied among the cells, we asked whether the half-width of the induced currents might correlate with the amplitude as a result of subtle variations in recording conditions. This hypothesis is not the case: When the half-width of the induced currents is plotted against the peak responses, there is no correlation for both lyral and high-K^+ responses (Fig. 3*E*). When fitted with the linear regression function, the correlation coefficient R is 0.22 with $P = 0.27$ (the probability that R is zero) for lyral responses and R is −0.10 with $P = 0.72$ for high-K^+ responses. A cell usually showed similar kinetics in responding to different odorants and to 3-isobutyl-1-methyl-xanthine, a blocker for phosphodiesterases (data not shown).

We measured the reversal potential for the odorant responses by holding the membrane potential at various levels; the averaged reversal potential from three cells was –7.9 mV (Fig. 4 *A* and *B*). Lyral was originally identified as an odorant that elevates the cellular inositol-1,4,5-trisphosphate (IP_3) level (22). Recent evidence indicates that the IP_3 pathway plays a modulatory role in cAMP signaling: LY294002, which blocks synthesis of IP_3 by inhibiting phosphoinositide 3-OH kinases, significantly enhanced odorant-induced calcium signals in a fraction of rat OSNs (23). We examined whether MOR23 cells employ these two pathways in responding to lyral. We observed a reversible, complete block of lyral-induced responses by 50 μM of MDL12330A, a potent inhibitor of adenylyl cyclase (Fig. 4*C*). In contrast, LY294002 (10 μM) did not have a significant effect on the responses (data not shown). Thus, lyral-induced responses in MOR23 cells are primarily, if not exclusively, mediated by the cAMP pathway (23, 24).

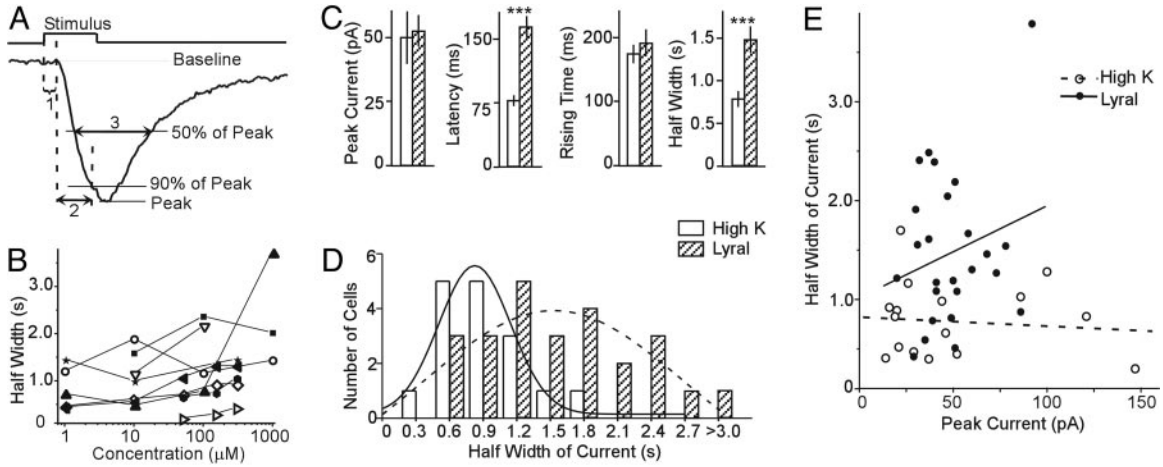

Fig. 3. Summary of lyral-induced responses in MOR23 cells. (*A*) Definition of the four parameters. The peak current is measured from the baseline to the peak. The response latency (*1*) is the time between the onset of the stimulus and the starting point of the response. The 0–90% rising time (*2*) is the time it takes for the current to reach 90% of the peak from the starting point of the response. The half-width of the current (*3*) is the time between the rising and falling phase at 50% of the peak. (*B*) The half-width of the transduction current is plotted against lyral concentration. The data were from nine cells with the holding potential of –50 mV. (*C*) Comparison between high-K^+ ($n = 16$) and lyral-induced responses ($n = 25$) in MOR23 cells. Data are shown in mean ± SE. Significant difference ($P < 0.001$, *t* test) is marked by ***. (*D*) Histogram of the distribution of the half-width of the currents induced by high K^+ and lyral, fitted by the Gaussian distributions. (*E*) The half-width of the induced current is plotted against the peak. The straight lines are linear regression fittings. Note that there is no correlation between the peak and the half-width.

Dose–Response Relationships. MOR23 cells responded to lyral in a dose-dependent manner. Under voltage clamp mode, lyral-induced inward currents increased with concentration (Fig. 5*A1*). The peak transduction currents versus the concentration from eight cells are plotted and fitted with the Hill equation, $I = I_{max}/(1 + (K_{1/2}/C)^n)$, where I represents the peak current, I_{max} the maximum response at saturating concentrations, $K_{1/2}$ the concentration at which half of the maximum response was reached, C the concentration of odorant and n the Hill coefficient (Fig. 5*A2*). I_{max} ranges from 22 to 91 pA and $K_{1/2}$ from 4.4 to 104 μM, indicating different sensitivities among MOR23 cells. This variability is also evident in the response thresholds of these cells. Some cells showed clear responses to lyral ≤0.1 μM (two of six cells responded to as little as 10 nM), whereas others did not respond at <10 μM, showing a difference in threshold of more than two orders of magnitude. With one exception (filled triangles in cyan, Fig. 5*A2*), the Hill coefficient of the dose–response curves is <1.5 with an average of 0.8 (from seven cells).

Under current clamp mode, lyral-induced receptor potentials (depolarization) in MOR23 cells also increased with concentration (Fig. 5*B*). Because mouse OSNs have a relatively high input resistance (≈4 GΩ; ref. 17), a small current would cause a large depolarization. On the other hand, the peak depolarization will not follow the peak transduction current linearly because of the reduced driving force under current clamp mode. Consequently, the peak depolarization showed a lower threshold and saturated at a lower concentration compared to the transduction current (Fig. 5 *B* and *C*). After the lyral-induced receptor potential reached its peak, it became longer-lasting when stimulated at higher concentrations (Fig. 5*B2 Inset*). As a result, the dose–response curves of the net depolarization, defined as the area under the receptor potential (mV × s), shifted to the right (Fig. 5 *B2* and *B3*). In the same cell, the peak depolarization saturated before the net depolarization and the peak transduction current (Fig. 5*C*). Thus, MOR23 cells respond to lyral with a broad dynamic range, which often covers ≈1,000-fold from threshold to saturation.

Discussion

We have here described the electrophysiological response properties of a population of mammalian OSNs that express the same endogenous OR. We have applied the perforated patch clamp technique in intact, nondissociated preparations of olfactory epithelium from MOR23-IRES-tauGFP gene-targeted mice. Although homogeneous for the expressed OR, MOR23 cells are heterogeneous in their response kinetics and sensitivity to lyral.

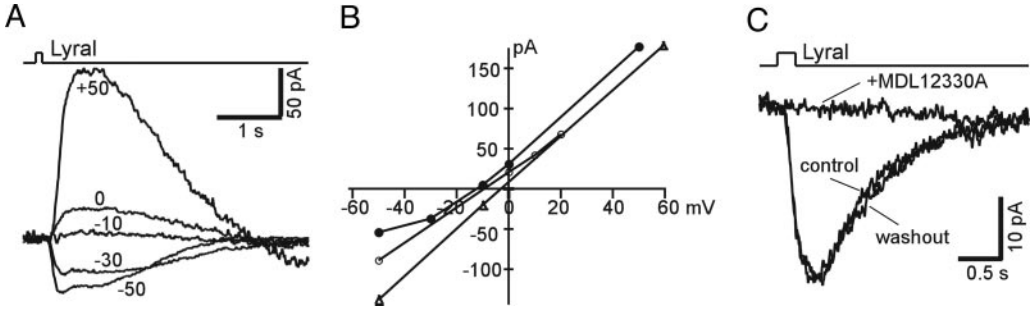

Fig. 4. Properties of lyral-induced responses in MOR23 cells. (*A* and *B*) The reversal potential of lyral-induced responses in the intact epithelium. (*A*) Lyral (10 μM) induced responses from a MOR23 cell at different holding potentials, indicated by the number next to each trace. The steady-state currents were subtracted. (*B*) The peak current is plotted against the holding potential for three different cells. (*C*) Lyral-induced responses were reversibly blocked by MDL12330A. The MOR23 cell was stimulated by 300 μM lyral, and the holding potential was −50 mV.

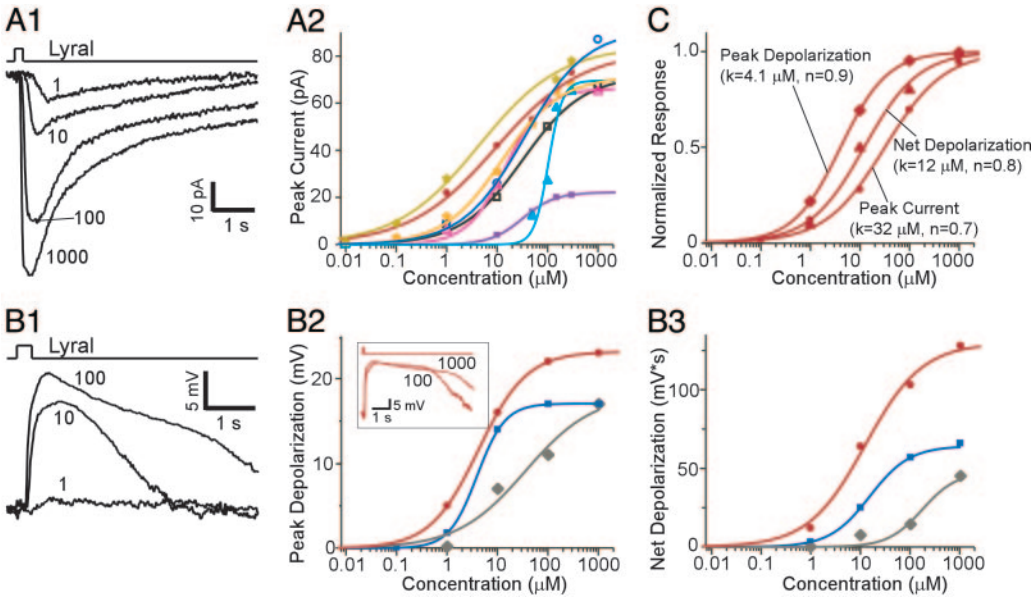

Fig. 5. Dose–response relationships of MOR23 cells in responding to lyral. (*A1*) The inward currents induced by lyral at different concentrations (indicated by the numbers in μM) under voltage clamp. The holding potential was −60 mV. (*A2*) The dose–response curves of the peak currents from eight cells fitted with Hill equations. (*B1*) Depolarization induced by lyral at different concentrations from another cell under current clamp. The resting potential was approximately −52 mV. (*B2* and *B3*) The dose–response curves of the peak depolarization (*B2*) or the net depolarization (*B3*) from three cells. (*B2 Inset*) The receptor potentials elicited by lyral at 100 and 1,000 μM in one cell (red) are shown. (*C*) The normalized three dose–response curves from the same cell. They are shown in filled circles in *A* and *B* (red). *K* represents the concentration when half of the maximum response was reached, and *n* is the Hill coefficient.

The response threshold varies 100-fold, and the concentration at which half of the maximum transduction current occurs varies 25-fold across the population of 53 cells examined. The dynamic range of individual MOR23 cells appears very broad, often across 1,000-fold of odorant concentrations from threshold to saturation. This approach offers a powerful means to study how peripheral inputs shape activity within individual glomeruli.

Odorant Responses of OSNs That Express the Same OR. The electrophysiological recording method used in this study offers several advantages over calcium imaging in isolated OSNs (14, 15). First, the recorded MOR23 cells are mature OSNs with intact cilia that are located in their normal configuration within the epithelium and covered with mucus (Fig. 1). The cells are not exposed to mechanical or enzymatic treatment, which is likely to be traumatic, particularly for the cilia where signal transduction occurs. Second, using the patch clamp technique, we measure the transduction currents and receptor potentials from the dendritic knobs, close to the cilia where signal transduction takes place. Arguably our method provides the most sensitive and accurate measurement of the electrical signals in olfactory transduction under an approximately physiological condition.

MOR23 cells show profound differences in the response kinetics of their electrophysiological responses to lyral. We noticed that high-K^+ responses show considerable variation among the cells in amplitude and half-widths. The delay of high-K^+ responses is ≈77 ms, which is much longer than the delay measured in puffing-induced junction potentials (≈30 ms; *Methods*). In contrast, high-K^+ induces instantaneous responses in isolated cells (25). The longer delay and variation of high K^+ responses observed here are likely due to the position of the cells at varying depths in the tissue and to the action of the mucus and epithelium as a diffusion barrier. Nevertheless, the deactivation phase of the high-K^+ responses can be fitted well by a single or double exponential curve, reflecting the withdrawal of the stimulus and the restoration to the original membrane parameters. In contrast, termination of the lyral responses is more complex and heterogeneous among MOR23 cells. Many cellular processes are involved in the deactivation of an odorant response, including deactivation of the transduction cascade, breakdown of cAMP by phosphodiesterases, and Ca^{2+}/calmodulin mediated inactivation of cyclic nucleotide-gated channels (26–32).

MOR23 cells also show differences in their sensitivity to lyral. Compared to neighboring cells, MOR23 cells are very sensitive to lyral. However, the sensitivity determined by the response threshold in individual cells can vary by at least 100-fold. Some cells showed clear responses to 10 nM, whereas others did not respond until 1 or 10 μM. This wide range of sensitivities is consistent with our previous study for acetophenone and benzaldehyde in M71 OSNs (14).

We can only speculate about the causes of the observed heterogeneity in response kinetics and odorant sensitivity. It cannot be excluded that the heterogeneity is, in part, caused by methodological factors, such as small, uncontrollable differences in experimental conditions and damage to the knob and cilia by the patch pipettes. We note that there is no control population of ''identical'' OSNs in which method-induced variability can be evaluated separately and measurements can be calibrated. But methodological factors cannot explain the observation that some cells with very similar ionic and leakage currents, which were closely monitored throughout each experiment (*Methods*), show profound differences in their deactivation phase, but not in their response amplitudes. In addition, odorant-induced responses vary more than high-K^+ responses do, indicating that the experimental conditions (puffing and recording) alone cannot account for this heterogeneity. A caveat in this study is that the perforated patch pipette contained a lower Cl^- concentration than that of OSNs (≈60 mM; ref. 33). This low Cl^- concentration may lead to underestimation of the Ca^{2+}-activated Cl^- component, which further amplifies the transduction signal carried by the cyclic nucleotide-gated channel (34, 35). However, this difference should not affect the main conclusions because all of the cells were recorded in the same way.

Several biological factors could potentially contribute to such heterogeneity. Intrinsic variations in levels of MOR23 mRNA or protein expression and in the number and size of cilia may contribute to the differences in odorant sensitivity and response amplitudes. The range in age of OSNs may affect their cellular properties: because of the asynchronous neurogenesis of OSNs, the age of the cells can vary from a few days to 12 weeks (the age of the oldest mice examined in this paper). Further, many cellular processes are involved in activation and deactivation of odorant-induced responses, and variations in these processes may be responsible for the heterogeneity in kinetics and sensitivity. It will be interesting to determine whether the heterogeneous responses of the converging OSNs can cause heterogeneity in patterns of intraglomerular activity (36).

Broad Dynamic Range of OSNs in the Intact Epithelium. In our experimental setup, MOR23 cells respond to lyral with a very broad dynamic range. In most cells, the responses, the transduction current, peak depolarization or net depolarization, do not saturate over a 100- to 1,000-fold increase of the concentration. These observations are in sharp contrast with the dose–response relationships of dissociated OSNs from salamander or mouse, where the transduction currents or the calcium signals saturate within one log unit (14, 37, 38). In isolated frog OSNs, a shallower dose–response curve was reported for the receptor current (≈2 log units) than for the firing frequency (≈1 log unit) (39). An important difference with the other electrophysiological studies (37–39) is that in our design, OSNs are homogeneous in terms of the expressed OR. It is unlikely but cannot be excluded that the very broad dynamic range is a special property of MOR23 cells or lyral. It is also unrelated to the recording condition (e.g., smaller Cl^- component), because similar curves are obtained by whole-cell patch clamp when the Cl^- equilibrium potential is ≈0 mV (unpublished data; ref. 17).

Several factors may contribute to a broad dynamic range. First, the role of the mucus in odorant reception may have been underestimated in the past. The mucus is very difficult to dissolve, even after repetitive washings (40). It contains complex components such as odorant binding proteins (OBPs; refs. 40–42), which may change the odorant concentrations that reach the cilia of the OSNs. When the odorant concentration is low, OBPs may help the odorant molecules to accumulate and deliver them to the cilia. But when the concentration is high, the mucus may act as a diffusion barrier and OBPs as buffers to reduce the concentration that reaches the cilia. In dissociated cell preparations (14, 37), it is likely that the mucus is more affected than in our intact epithelium preparation. Second, supporting cells may help to balance various ionic concentrations during odorant responses (43, 44) and reduce the possibility of saturation. Third, recording from the dendritic knobs, near the cilia, may enable the detection of small transduction signals elicited by weak stimuli. Thus, the observed dose–response relationships may reflect to some extent the peri-receptor events in addition to the properties of OR binding and signal amplification. Obviously, what matters *in vivo* is the totality of these events, not only the odorant–OR interaction.

It will be interesting to determine how the transduction currents or receptor potentials in MOR23 cells are transformed into action potentials (45) that carry the information to the next stage, the glomerulus where the OSN axons synape with the second-order neurons in the olfactory pathway. Under current clamp mode, we observed action potentials in some cells, but not all of them (data not shown); we cannot completely rule out a methodological factor for the lack of consistency. But it is also possible that the action potentials are generated relatively far out in the axon, and that they do not backpropagate into the soma and dendrites, for the following two reasons. First, the receptor potentials are high enough (due to high-input resistances and large transduction currents) to inactivate local sodium channels, perhaps preventing firing at the dendrites and soma. Second, the OSNs have very thin, unmyelinated axons, which cause a large impedance mismatch between the axon and soma-dendrites, perhaps preventing backpropagation of action potentials. The broad dose–response relationships, combined with the variation of the odorant sensitivity of OSNs that express the same OR, could potentially make the glomeruli responsive to a particular odorant over a relatively wide dynamic range (10).

Methods

Preparations. The mouse strain MOR23-IRES-tauGFP, in which cells expressing the OR MOR23 are tagged with tauGFP, has been described in detail in ref. 19. Line 7162 was used, in a mixed 129 × B6 background. Mice were between 4 and 12 weeks of age; ≈80% of mice were between 4 and 6 weeks. The procedure for the intact epithelial preparations has been described in refs. 17 and 18. Mice were deeply anesthetized by injection of ketamine and decapitated. The head was immediately put into icy Ringer's solution, which contained 124 mM NaCl, 3 mM KCl, 1. 3 mM $MgSO_4$, 2 mM $CaCl_2$, 26 mM $NaHCO_3$, 1.25 mM NaH_2PO_4, and 15 mM glucose (pH 7.6 and 305 mOsm). The nose was dissected out *en bloc*. The olfactory epithelium attached to the nasal septum and the dorsal recess were removed and kept in oxygenated Ringer's solution. Before the recording, the epithelium was peeled off from the underlying bone as a whole and transferred to a recording chamber with the mucus layer facing up, and the oxygenated Ringer's solution was continuously perfused at 25 ± 2°C.

Patch Clamp. The dendritic knobs of OSNs were visualized through an upright DIC microscope (Olympus BX50WI) equipped with a charge-coupled device camera (Dage-MTI) and a ×40 water-immersion objective. An extra ×4 magnification was achieved by using a magnification changer (Luigs and Neumann, Ratingen, Germany). The GFP-tagged MOR23 cells were visualized under fluorescent illumination. Superimposition of the fluorescent and DIC images allowed identification of the GFP^+ cells under the DIC image, which directed the recording pipettes. Perforated patch clamp was performed on the dendritic knobs by including 260 μM amphotericin B or nystatin in the recording pipette, which was filled with the solution containing 17.7 mM KCl, 105.3 mM KOH (pH 7.2), 82.3 mM methanesulfonic acid, 5.0 mM EGTA, 10 mM Hepes, and 70 mM sucrose (310 mOsm) (46). Repeated *I–V* tests (measuring the ionic currents elicited by voltage steps, 10–90 mV from the holding potential) were performed after formation of the Gigaohm seal. Full electrical access to the cells was established when no further changes in the ionic currents occurred. Such *I–V* tests were frequently performed between the odorant responses to ensure consistency in the electrical access. Electrophysiological recordings were controlled by an EPC-9 amplifier combined with the PULSE software (HEKA Electronic, Lambrecht, Germany). The response kinetics was analyzed by using the HEKA PULSEFIT software.

Odorant Stimulation. A multibarrel pipette, placed ≈20 μm downstream from the recording site, was used to deliver stimuli by pressure ejection through a Picospritzer (General Valve, Fairfield, NJ). The recorded cell was always positioned in the center on the screen, with the puffing pipette on the edge. Odorants were dissolved at 0.5 M in dimethyl sulfoxide (DMSO) and kept at −20°C. Final solution was prepared before each experiment by adding Ringer's solution. Because the concentration that reaches the cilia may depend on the position of the cell and the pulse pressure and length, we performed three sets of controls to ensure that the cells were appropriately stimulated by what was inside the pipettes.

In the first set of experiments, a recording electrode filled with Ringer's solution was used to measure the junction potentials induced by 3 M KCl solution included in the puffing pipettes (three seven-barrel pipettes were tested). The junction potentials followed the puffs (20 psi or 138 KPa) with a delay of ≈30 ms and reached the maximum value at 200–300 ms (varied slightly from different barrels). When the pressure was increased from 5 to 20 psi, the onset became faster and the junction potential plateaus increased with the pressure. When the pressure was >20 psi, the junction potential plateaus stayed constant, even though the onset was slightly faster with increased pressure. We kept the pressure at ≈20 psi in all experiments. In the second set, odorant concentrations were estimated at various positions from the light intensity changes when blue food colors were delivered from the multibarrel pipettes. We took a series of time lapse images by using a cooled charge-coupled device camera (SensiCam QE; Cooke Corporation, Romulus, MI) and METAMORPH software (Molecular Devices), and we varied the pulse length from 50 ms to 2 s. The light intensities were measured in a series of circles (10 μm in diameter) with increased distance from the source. The light attenuation reached its maximum at ≈300 ms in all positions. Even though the light change gradually decreased with increased distance from the center of the "bolus" (located at ≈30 μm from the source), the effect of the food color was nearly uniform within a diameter of ≈70 μm. This observation suggests that all of the cilia (≈10 μm long) of a single cell should be stimulated evenly. In our perfusion system, when the pulse ranges from 0.2 to 1 s, the food dye is cleared away consistently with a time constant of 0.8–0.9 s. In the third set of experiments, a series of pulses with different length (10–300 μM lyral) were delivered to six MOR23 cells. When the pulse length was increased from 5 ms to 2 s, the peak of the transduction currents increased until the pulse reached 200 ms, and there was no further increase with longer pulses. Therefore, we chose to use odorant pulses of 200–300 ms in most of the experiments.

High-K^+ solution replaced 100 mM Na^+ with K^+ in Ringer's solution. 3-isobutyl-1-methyl-xanthine was prepared in a 20 mM stock solution containing 5% DMSO and diluted to the final concentrations before use. MDL12330A was diluted by adding Ringer's solution before each experiment. All compounds and chemicals were obtained from Sigma-Aldrich, except for lyral [3-cyclohexene-1-carboxaldehyde, 4-(4-hydroxy-4-methyl pentyl)], which was generously provided by Kazushige Touhara (University of Tokyo, Tokyo).

We thank Dr. Tom Bozza for critical reading of the manuscript. This work was supported by National Institute on Deafness and Other Communication Disorders/National Institutes of Health grants (to M.M., G.M.S., A.V., and P.M.) and by the Whitehall Foundation (M.M.).

1. Buck, L. & Axel, R. (1991) *Cell* **65,** 175–187.
2. Young, J. M., Shykind, B. M., Lane, R. P., Tonnes-Priddy, L., Ross, J. A., Walker, M., Williams, E. M. & Trask, B. J. (2003) *Genome Biol.* **4,** R71.
3. Zhang, X., Rogers, M., Tian, H., Zou, D.-J., Liu, J., Ma, M., Shepherd, G. M. & Firestein, S. J. (2004) *Proc. Natl. Acad. Sci. USA* **101,** 14168–14173.
4. Ressler, K. J., Sullivan, S. L. & Buck, L. B. (1994) *Cell* **79,** 1245–1255.
5. Vassar, R., Chao, S. K., Sitcheran, R., Nunez, J. M., Vosshall, L. B. & Axel, R. (1994) *Cell* **79,** 981–991.
6. Mombaerts, P., Wang, F., Dulac, C., Chao, S. K., Nemes, A., Mendelsohn, M., Edmondson, J. & Axel, R. (1996) *Cell* **87,** 675–686.
7. Treloar, H. B., Feinstein, P., Mombaerts, P. & Greer, C. A. (2002) *J. Neurosci.* **22,** 2469–2477.
8. Rubin, B. D. & Katz, L. C. (1999) *Neuron* **23,** 499–511.
9. Johnson, B. A., Woo, C. C., Hingco, E. E., Pham, K. L. & Leon, M. (1999) *J. Comp. Neurol.* **409,** 529–548.
10. Wachowiak, M. & Cohen, L. B. (2001) *Neuron* **32,** 723–735.
11. Schaefer, M. L., Young, D. A. & Restrepo, D. (2001) *J. Neurosci.* **21,** 2481–2487.
12. Xu, F., Kida, I., Hyder, F. & Shulman, R. G. (2000) *Proc. Natl. Acad. Sci. USA* **97,** 10601–10606.
13. Bozza, T., McGann, J. P., Mombaerts, P. & Wachowiak, M. (2004) *Neuron* **42,** 9–21.
14. Bozza, T., Feinstein, P., Zheng, C. & Mombaerts, P. (2002) *J. Neurosci.* **22,** 3033–3043.
15. Feinstein, P., Bozza, T., Rodrigues, I., Vassalli, A. & Mombaerts, P. (2004) *Cell* **117,** 833–846.
16. Mombaerts, P. (2004) *Nat. Rev. Neurosci.* **5,** 263–278.
17. Ma, M., Chen, W. R. & Shepherd, G. M. (1999) *J. Neurosci. Methods* **92,** 31–40.
18. Ma, M. & Shepherd, G. M. (2000) *Proc. Natl. Acad. Sci. USA* **97,** 12869–12874.
19. Vassalli, A., Rothman, A., Feinstein, P., Zapotocky, M. & Mombaerts, P. (2002) *Neuron* **35,** 681–696.
20. Touhara, K., Sengoku, S., Inaki, K., Tsuboi, A., Hirono, J., Sato, T., Sakano, H. & Haga, T. (1999) *Proc. Natl. Acad. Sci. USA* **96,** 4040–4045.
21. Firestein, S. (2001) *Nature* **413,** 211–218.
22. Boekhoff, I., Tareilus, E., Strotmann, J. & Breer, H. (1990) *EMBO J.* **9,** 2453–2458.
23. Spehr, M., Wetzel, C. H., Hatt, H. & Ache, B. W. (2002) *Neuron* **33,** 731–739.
24. Chen, S., Lane, A. P., Bock, R., Leinders-Zufall, T. & Zufall, F. (2000) *J. Neurophysiol.* **84,** 575–580.
25. Firestein, S. & Werblin, F. (1989) *Science* **244,** 79–82.
26. Boekhoff, I. & Breer, H. (1992) *Proc. Natl. Acad. Sci. USA* **89,** 471–474.
27. Boekhoff, I., Inglese, J., Schleicher, S., Koch, W. J., Lefkowitz, R. J. & Breer, H. (1994) *J. Biol. Chem.* **269,** 37–40.
28. Borisy, F. F., Ronnett, G. V., Cunningham, A. M., Juilfs, D., Beavo, J. & Snyder, S. H. (1992) *J. Neurosci.* **12,** 915–923.
29. Yan, C., Zhao, A. Z., Bentley, J. K., Loughney, K., Ferguson, K. & Beavo J. A. (1995) *Proc. Natl. Acad. Sci. USA* **92,** 9677–9681.
30. Kramer, R. H. & Siegelbaum, S. A. (1992) *Neuron* **9,** 897–906.
31. Varnum, M. D. & Zagotta, W. N. (1997) *Science* **278,** 110–113.
32. Wei, J., Zhao, A. Z., Chan, G. C., Baker, L. P., Impey, S., Beavo, J. A. & Storm, D. R. (1998) *Neuron* **21,** 495–504.
33. Kaneko, H., Putzier, I., Frings, S., Kaupp, U. B. & Gensch, T. (2004) *J. Neurosci.* **24,** 7931–7938.
34. Kurahashi, T. & Yau, K. W. (1993) *Nature* **363,** 71–74.
35. Lowe, G. & Gold, G. H. (1993) *Nature* **366,** 283–286.
36. Wachowiak, M., Denk, W. & Friedrich, R. W. (2004) *Proc. Natl. Acad. Sci. USA* **101,** 9097–9102.
37. Firestein, S., Picco, C. & Menini, A. (1993) *J. Physiol. (London)* **468,** 1–10.
38. Reisert, J. & Matthews, H. R. (2001) *J. Physiol. (London)* **530,** 113–122.
39. Reisert, J. & Matthews, H. R. (1999) *J. Physiol. (London)* **519,** 801–813.
40. Pelosi, P. (1996) *J. Neurobiol.* **30,** 3–19.
41. Getchell, T. V., Margolis, F. L. & Getchell, M. L. (1984) *Prog. Neurobiol.* **23,** 317–345.
42. Steinbrecht, R. A. (1998) *Ann. N.Y. Acad. Sci.* **855,** 323–332.
43. Trotier, D. & MacLeod, P. (1986) *Brain Res.* **374,** 205–211.
44. Trotier, D. (1998) *Chem. Senses* **23,** 363–369.
45. Tomaru, A. & Kurahashi, T. (2005) *J. Neurophysiol.* **93,** 1880–1888.
46. Zufall, F. & Leinders-Zufall, T. (1997) *J. Neurosci.* **17,** 2703–2712.